Hydrology and Earth System Sciences, 4(3), *463–482* (2000) © EGS

Hydrology & Earth System Sciences

Climatic and basin factors affecting the flood frequency curve: PART I—A simple sensitivity analysis based on the continuous simulation approach

A.M. Hashemi[1], M. Franchini[2] and P.E. O'Connell[1]

[1]University of Newcastle upon Tyne, Department of Civil Engineering, Cassie Building, NE1 7RU, UK
[2]Università degli Studi di Ferrara, Dipartimento di Ingegneria, Via Saragat 1, I-44100 Ferrara (I)
e-mail for corresponding authors: mfranchini@ing.unife.it; ahmad.moaven-hashemi@ncl.ac.uk; P.E.O'Connell@ncl.ac.uk

Abstract

Regionalized and at-site flood frequency curves exhibit considerable variability in their shapes, but the factors controlling the variability (other than sampling effects) are not well understood. An application of the Monte Carlo simulation-based derived distribution approach is presented in this two-part paper to explore the influence of climate, described by simulated rainfall and evapotranspiration time series, and basin factors on the flood frequency curve (ffc). The sensitivity analysis conducted in the paper should not be interpreted as reflecting possible climate changes, but the results can provide an indication of the changes to which the flood frequency curve might be sensitive.

A single site Neyman Scott point process model of rainfall, with convective and stratiform cells (Cowpertwait, 1994; 1995), has been employed to generate synthetic rainfall inputs to a rainfall runoff model. The time series of the potential evapotranspiration (ETp) demand has been represented through an AR(n) model with seasonal component, while a simplified version of the ARNO rainfall-runoff model (Todini, 1996) has been employed to simulate the continuous discharge time series. All these models have been parameterised in a realistic manner using observed data and results from previous applications, to obtain 'reference' parameter sets for a synthetic case study. Subsequently, perturbations to the model parameters have been made *one-at-a-time* and the sensitivities of the generated annual maximum rainfall and flood frequency curves (unstandardised, and standardised by the mean) have been assessed.

Overall, the sensitivity analysis described in this paper suggests that the soil moisture regime, and, in particular, the *probability distribution of soil moisture content at the storm arrival time*, can be considered as a unifying link between the perturbations to the several parameters and their effects on the standardised and unstandardised ffcs, thus revealing the physical mechanism through which their influence is exercised. However, perturbations to the parameters of the linear routing component affect only the unstandardised ffc.

In Franchini *et al.* (2000), the sensitivity analysis of the model parameters has been assessed through an analysis of variance (ANOVA) of the results obtained from a formal experimental design, where all the parameters are allowed to vary *simultaneously*, thus providing deeper insight into the interactions between the different factors. This approach allows a wider range of climatic and basin conditions to be analysed and reinforces the results presented in this paper, which provide valuable new insight into the climatic and basin factors controlling the ffc.

Keywords: stochastic rainfall model; rainfall runoff model; simulation; derived distribution; flood frequency; sensitivity analysis

Introduction

Regional flood frequency analysis has now evolved into a robust and mature methodology for estimating the T-year flood at both gauged and ungauged sites (Hosking and Wallis, 1997). A key element of this methodology is the choice of homogeneous groups of catchments for regionalisation, and it is now accepted that this should be based on similarity criteria rather than geographical proximity. Developments in information technology have greatly facilitated this process (Institute of Hydrology, 1999). However, regardless of which approach is used to define homogeneous groups, the resulting sets of flood frequency curves still exhibit considerable variation between regions (NERC, 1975; Farquharson *et al.*, 1992; Hosking and Wallis, 1997). Although sampling variability doubtless contributes to this variation, climatic and basin factors must account for much of it. How important is the influence of climate, reflected primarily by the rainfall and evapotranspiration regimes which jointly control soil moisture, in comparison with basin factors, and how do these interact to determine the basin flood frequency curve (ffc)? This is the

rationale for the research reported here which employs a simulation model-based derived distribution approach to assessing the impacts of climatic and basin factors on the ffc.

The derived distribution approach has its origins in the pioneering work of Eagleson (1972) who proposed a physically-based analytical framework for deriving a basin flood frequency distribution. Further analytical work has been reported by Hebson and Wood (1982), Wood and Hebson (1986), Diaz-Granados *et al.* (1984), Adom *et al.* (1989), Shen *et al.* (1990) and Cadavid *et al.* (1991). Recently, Fiorentino and Jacobellis (2000) and Jacobellis and Fiorentino (2000) have developed a physically-based analytical framework in which interactions between climate, runoff production and the ffc are accounted for. Their work suggests that climate and basin factors exercise a strong control on the ffc.

Applications of a Monte Carlo simulation-based derived distribution approach, in which a stochastic model of rainfall is linked with a rainfall-runoff model, have been described by Franchini *et al.* (1996), Blazkova and Beven (1997) and Cameron *et al.* (2000). Hashemi *et al.* (1998) have linked a generalised point process model of rainfall with a simplified version of the ARNO model (Todini, 1996) to carry out a limited simulation analysis of the factors controlling the ffc. The results of this preliminary work also suggest that climate, represented by variations in rainfall and potential/actual evapotranspiration, and basin factors appear to exercise strong controls on the ffc.

However, it should be emphasized that the purpose of the work performed here is not to explore the influence of possible climatic and basin changes on the flood frequency curve. Such an analysis would need to consider, for example, changes induced in the biosphere, in vegetation growth and extent, in land use *etc.*, and that is not the objective of the work reported here. Rather, the sensitivity analysis has been designed to reveal why a flood frequency curve has a particular shape by identifying the factors controlling that shape. However, the results of the sensitivity analysis might be used to infer the influence of climatic changes on the ffc.

In this two-part paper, the Monte-Carlo simulation derived distribution framework proposed by Hashemi *et al.* (1998) is used to carry out a comprehensive sensitivity analysis (*SA*) of a range of climatic and basin factors which might exert controls on the ffc; these are represented by the parameters of the rainfall, potential evapotranspiration and rainfall-runoff models. In this paper, a simple form of *SA* is employed in which the parameters are perturbed *one-at-a-time* from a reference set of values, and the influence on the ffc assessed through graphical probability plots and L-moments, for both unstandardised and standardised distributions. In Franchini *et al.* (2000), a more rigorous *SA* approach is employed in the form of a factorial experiment combined with the analysis of variance (ANOVA) technique which accounts for interactions between the model parameters and which also allows the statistical significance of different effects, due to one or more parameters, to be tested.

Description of the simulation models used for the sensitivity analysis

STOCHASTIC RAINFALL MODEL

A single site Neyman Scott point process model of rainfall, with two types of cells termed convective (high intensity and short duration) and stratiform (low intensity and long duration), has been employed to generate synthetic rainfall inputs to the rainfall runoff model. This is a special case of the GNSRP model (Cowpertwait, 1994, 1995) and is designated as GNSRP(2) to represent two cell types. Following Cowpertwait (1994), let storm origins occur in a Poisson process of rate λ, each origin generating a random number N of rain cell origins on the basis of a geometric distribution with parameter v. The cell origins are independently displaced from the storm origin by distances that are exponentially distributed with parameter β, no cell origin being located at the storm origin. Each cell origin is classified as one of two types, with α denoting the probability of a convective cell. A rectangular pulse is associated with each cell origin; the duration of the pulse is assumed to be an independent exponential random variable with parameter η_i ($i = 1$: convective or heavy cell, $i = 2$: stratiform or light cell); also, the intensity of each pulse is taken to be an independent exponential random variable with parameter ξ_i with i equal to 1 or 2 according to the cell type. The GNSRP(2) model has therefore a total of 8 parameters which are summarised in Table 1.

STOCHASTIC POTENTIAL EVAPOTRANSPIRATION MODEL

The time series of the potential evapotranspiration (*ETp*)

Table 1. Description of the parameters of the GNSRP(2) rainfall model.

Symbol	Description
λ^{-1}	average time between two subsequent storm arrivals
v^{-1}	average number of cells per storm
β^{-1}	average time between storm and cell origin
α	probability or fraction of the convective cells (type 1) within a storm
η_1^{-1}	average duration of a convective cell (type 1)
η_2^{-1}	average duration of a stratiform cell (type 2)
ξ_1^{-1}	average intensity of a convective cell (type 1)
ξ_2^{-1}	average intensity of a stratiform cell (type 2)

demand was represented through an AR(n) model with seasonal component. More precisely, let $x_{i,j}$ be the ETp demand of the ith time step of the jth year, and $z_{i,j}$ be the corresponding standardised quantity without periodicity, i.e.

$$z_{i,j} = \alpha_1 z_{i-1,j} + \alpha_2 z_{i-2,j} + \ldots + \alpha_n z_{i-n,j} + \varepsilon_i \qquad (1a)$$

where

$$z_{i,j} = \frac{x_{i,j} - \mu_k}{\sigma_k} \qquad (1b)$$

where μ_k and σ_k are the mean and the standard deviation valid for the whole kth month, respectively, α_i are autoregressive coefficients and ε_i represents white Gaussian noise.

RAINFALL-RUNOFF MODEL

A simplified version of the lumped ARNO rainfall-runoff model (Todini, 1996) was employed to simulate flood frequency curves using the generated rainfall and potential evapotranspiration inputs. The model selected characterises the rainfall-runoff process into two distinct components: a runoff production component and a runoff routing component (Fig. 1). Following the approach of Zhao (1977), a distribution function is used to represent soil moisture storage capacity across the catchment. This function is (see also Todini, 1996):

$$\frac{A}{A_T} = 1 - \left(1 - \frac{w}{w_{\max}}\right)^b = 1 - \left[\left(1 - \frac{W_o}{W_m}\right)^{\frac{1}{b+1}}\right]^b \qquad (2)$$

where A/A_T represents the fraction of the saturated area, w is the 'point/local' storage capacity, $w_{\max}$ is the *maximum* 'point/local' storage capacity, W_o is the *average* (over the basin) current soil moisture, while W_m and b are two parameters, the former representing the basin *average* value of the 'point/local' storage capacities (referred to subsequently as the *soil moisture storage capacity*), and the latter a parameter which controls the shape of the distribution function. These latter parameters are linked to each other

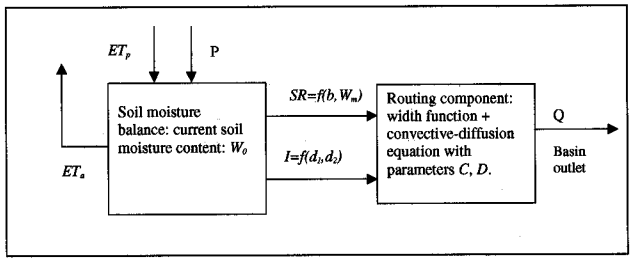

Fig. 1. *Scheme of the simplified rainfall runoff model; SR – surface runoff; I – interflow; P – precipitation; ET_p – potential evapotranspiration; ETa – actual evapotranspiration; Q – discharge.*

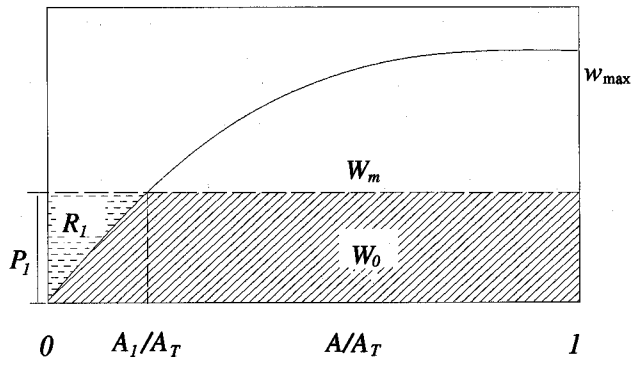

Fig. 2. *Schematic representation of the surface runoff mechanism based on the soil storage capacity distribution (after Zhao, 1977). P_1 – rainfall depth; W_o current soil moisture i.e. average depth of the water stored in the soil; W_m – soil moisture storage capacity (total area under the curve); w_{max} – maximum point storage capacity; A_1/A_T proportion of the basin area A_T in a saturated condition due to P_1; R_1 – surface runoff due to P_1.*

through the following equation (Zhao, 1977):

$$W_m = \frac{w_{\max}}{b+1} \qquad (3)$$

which implies that an increment of W_m produces a decrement of b when $w_{\max}$ is kept constant.

Surface runoff is produced in the model according to the Dunne saturation excess mechanism. Figure 2 gives an example of how the surface runoff is computed for an assigned rainfall depth P_1. For more details the reader can refer to Todini (1996).

An interflow component of the form:

$$I = d_1 \left(\frac{W_o}{W_m}\right)^{d_2} \qquad (4)$$

was used to describe subsurface flow I; d_1 and d_2 are parameters (Franchini, 1996) (see also Table 2). Percolation to groundwater and a base flow component were disregarded, in comparison with the full ARNO model formulation, mainly to keep the number of parameters small, and thus focus attention on basins where the flow at the outlet is due mainly to interflow and surface runoff components.

The actual evapotranspiration ETa was calculated as:

$$ETa = ETp \qquad \text{if } W_o > \gamma \cdot W_m;$$
$$ETa = ETp\left(\frac{W_o}{\gamma \cdot W_m}\right) \qquad \text{if } W_o \le \gamma \cdot W_m \qquad (5)$$

where ETp is the potential evapotranspiration input to the model. With this relationship, the ratio (ETa/ETp) decreases linearly with (W_o/W_m) below a threshold γ, which, for the present study, was taken as 0.75.

Finally, the routing component employed here differed

Table 2. Description of the parameters of the rainfall-runoff model.

Water balance component	
Surface runoff	
b	Shape parameter of the storage capacity distribution curve
W_m	Soil moisture storage capacity
Interflow	
d_1	Maximum interflow rate
d_2	Shape parameter of the interflow curve
Routing Component	
C, D	Convectivity and Diffusivity respectively of the parabolic model for routing runoff to the basin outlet

from that described by Todini (1996) and consisted of a network width function and linear convective-diffusion transfer function with parameters C and D for channel routing (Naden 1992; Franchini and O'Connell, 1996). The parameter C is the celerity i.e. the velocity of a discharge perturbation, and it controls the average arrival time of a flood wave at the basin outlet. The parameter D is the diffusivity and its value directly controls the attenuation of the flood wave moving downstream.

These simplifications enabled us to explore the sensitivity of the flood frequency curve to a reduced set of six rainfall runoff model parameters (soil moisture balance: parameters W_m, b, d_1, d_2; linear channel routing: parameters C and D) (see Table 2) and to channel network length and shape.

Reference parameter sets

The models previously described have to be parameterised in a reasonable manner in order to make the model-based sensitivity analysis as physically realistic as possible, thus allowing interpretations of wide validity to be extracted from the results. In the following sections, the procedures used to define the 'reference parameter sets' of the three models are described.

GNSRP(2) RAINFALL MODEL

The reference parameter set was identified by applying the parameterisation technique proposed by Cowpertwait (1994) to a site (Manston) in the south east of the UK with a 24 year hourly rainfall record and annual average rainfall of 560 mm which is distributed fairly uniformly throughout the year. In particular, the model is fitted to each calendar month of an hourly rainfall record in order to take account of seasonality. Thus, 12 monthly estimates per parameter are needed to give a total of 96 estimates for the site. When estimating the parameters, very little seasonality was observed for the parameters β, η_1 and η_2 and thus a constant value for each of them was assumed and the parameterisation process repeated.

The set of estimated parameters for the Manston site is presented in Table 3. The parameter estimates take physically realistic values. Over the summer months, the rate of storm arrival (λ) decreases, the proportion of the

Table 3. Rainfall model parameters for the rainfall station in Manston and the perturbation applied to each of them.

Month	λ *1/h*	ν *storm/cell*	β *1/h*	α	η_1 *1/h*	η_2 *1/h*	ξ_1 *h/mm*	ξ_2 *h/mm*
Jan	0.030	0.382	0.24	0.14	3.50	0.53	0.26	2.48
Feb	0.027	0.487	0.24	0.13	3.50	0.53	0.26	2.22
Mar	0.027	0.470	0.24	0.11	3.50	0.53	0.26	1.92
Apr	0.024	0.483	0.24	0.18	3.50	0.53	0.26	1.79
May	0.025	0.500	0.24	0.47	3.50	0.53	0.26	1.61
Jun	0.019	0.369	0.24	0.50	3.50	0.53	0.23	1.51
Jul	0.015	0.407	0.24	0.50	3.50	0.53	0.22	0.80
Aug	0.011	0.318	0.24	0.50	3.50	0.53	0.13	1.02
Sep	0.012	0.382	0.24	0.50	3.50	0.53	0.26	0.41
Oct	0.021	0.298	0.24	0.50	3.50	0.53	0.24	1.57
Nov	0.030	0.389	0.24	0.22	3.50	0.53	0.26	1.61
Dec	0.026	0.403	0.24	0.14	3.50	0.53	0.26	1.87
Perturbation	+/−25%	+/−25%	+/−25%	+/−25%	+/−25%	+/−25%	+/−25%	+/−25%

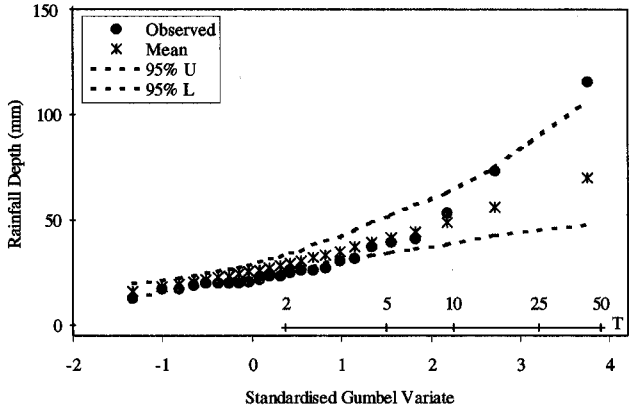

Fig. 3. *Observed 12 h annual maximum rainfalls for Manson together with 5 and 95 percentiles obtained from an ensemble of 100 synthetic series of length 24 years.*

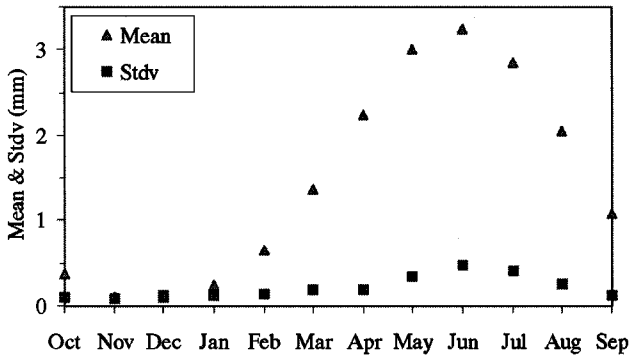

Fig. 4. *Seasonal behaviour of the monthly means and standard deviations for the historical series of potential evapotranspiration recorded for the upper Thames catchment.*

heavy cells (α) increases and also their expected intensity increases (see Table 3). Thus, the summer storms generated by the model will be heavier and contain more convective rainfall than the winter storms. This agrees with the physical interpretation that summer rainfall for a site in the South of the UK (Manston) is characterized by more heavy convective storms than winter rainfall.

However, these considerations are relevant to the *overall* behaviour of the GNSRP(2) model, while particular importance is attached here to the ability of the model to reproduce the observed behaviour of rainfall *extremes* for different durations. For this reason a validation analysis of the extremes was performed. The observed annual maximum rainfall depths over different durations (1, 3, 6, 12, 24 h) were extracted from the historical hourly time series, ordered and plotted against the standardised Gumbel variate (Fig. 3). Then, using the historical parameter estimates (Table 3) an ensemble of 100 time series of length 24 years was simulated and the annual maximum totals for the specified durations extracted; the 5 and 95 percentiles are plotted with the observed data as in Fig. 3, which refers to a duration of 12 h. The historic extremes lie within the bounds, and, allowing for sampling variability, the extremes generated by the model are consistent with the historical values. Similar plots are obtained for the other rainfall durations. Therefore, the parameter estimates for Manston were used as the reference set for the GNSRP(2) model.

POTENTIAL EVAPOTRANSPIRATION MODEL

The model was calibrated by using an observed time series of *daily* data recorded over the period 1 October 1951–30 September 1976 for a site located in the upper Thames catchment in the South of England. Figure 4 represents the seasonal behaviour of the monthly means and standard deviations of the daily evapotranspiration values. The AR(n) model was calibrated on the standardised series whose partial autocorrelation function suggested the use of an order $n = 3$, thus obtaining:

$$\hat{z}_{i,j} = 0.82\hat{z}_{i-1,j} + 0.01\hat{z}_{i-2,j} + 0.12z_{i-3,j} + \varepsilon_i \qquad (7)$$

An analysis of the residual terms ε_i has shown a good agreement with the normal distribution.

The daily data generated by the model described above were disaggregated to the hourly level using a sine-cosine wave. The generated hourly values were assumed to be independent from the generated hourly rainfall data. This assumption is supported by a generally weak observed correlation between hourly potential evapotranspiration and rainfall data.

The generated time series thus obtained was considered as the *reference* potential evapotranspiration demand *ETp* at the basin level.

RAINFALL-RUNOFF MODEL

In order to define the reference parameter set for the rainfall runoff model, the parameter sets for several previous applications of the ARNO model were reviewed (see, for example, Todini, 1996; Franchini *et al.*, 1996; Anselmo *et al.*, 1996), and a reference set was selected (see Table 4) on the basis of the most frequent values observed for each parameter. This approach was adopted to avoid having a reference set biased to one particular catchment, thus leaving the sensitivity analysis to reveal the effect of the soil moisture capacity, drainage rate, routing component *etc.*, on the ffc characteristics.

For the remaining two characteristics of a basin necessary to run the model, i.e. the width function and the area, the symmetric width function, labelled WF_{ref} in Fig. 5, was adopted which has a base length consistent with a basin area set to a value of 100 km^2. Although the width functions of real drainage networks are usually slightly negatively skewed, a symmetric shape was selected for the reference case, thus leaving the sensitivity analysis to reveal, as for the

Table 4. Reference set, upper and lower values for the rainfall-runoff model parameters.

Parameter	Lower value (−)	Reference value	Upper value (+)
W_m [mm]	50	150	250
b	0.05	0.15	0.3
d_1 [mm/h]	0.04	0.08	0.12
d_2	5.0	10	15.0
C [m/s]	0.2	0.5	0.8
D [m^2/s]	100	1000	5000

runoff production component, the effect of different width function shapes and base lengths on the flood frequency curve. However, the basin area was kept at 100 km^2 in view of the lumped nature of the rainfall runoff model used which does not allow for a representation of the spatial variation of the rainfall.

Sensitivity analysis of the flood frequency distribution

GENERATION OF SYNTHETIC DISCHARGE SERIES

The sensitivity analysis has been carried out with the GNSRP(2), potential evapotranspiration and rainfall runoff model parameters in the following way. Continuous hourly time series of rainfall and potential evapotranspiration, of length 10000 years, were generated using the reference parameter sets for both models. These time series, which were assumed to represent basin average values, were used as inputs to the rainfall runoff model, and an hourly time series of discharges was generated. Then, the annual maximum flood peaks were extracted, ordered and plotted against the Gumbel variate. Subsequently, perturbations, i.e. changes to the values of the several parameters, were made *one-at-a-time* and the sensitivities of the generated annual maximum rainfall (for durations $d = 1$, 6 and 12 h) and flood frequency curves were assessed graphically and with the assistance of the following quantities derived from each synthetic series:

(a) mean (m), L-coefficient of variation (L-CV) and L-coefficient of skewness (L-CS) (Hosking and Wallis, 1997) for the rainfall and flood annual maximum values; for the rainfall data, the subscript R, d is used, e.g. $m_{R,1}$, $m_{R,6}$, *etc.*, while for the discharge the subscript Q is used, e.g. m_Q; note that the mean m_Q describes the 'location' of the flood frequency curve, while L-CS_Q describes its curvature (shape);

(b) annual average precipitation (AVP), actual evapotranspiration (AVE), surface runoff ($AVSR$), interflow (AVI) and total runoff ($AVRF$). The percentages of AVE, $AVSR$, AVI and $AVRF$ with respect to AVP were also considered; the ratio $AVRF/AVP$ represents the annual average runoff coefficient $AVRC$.

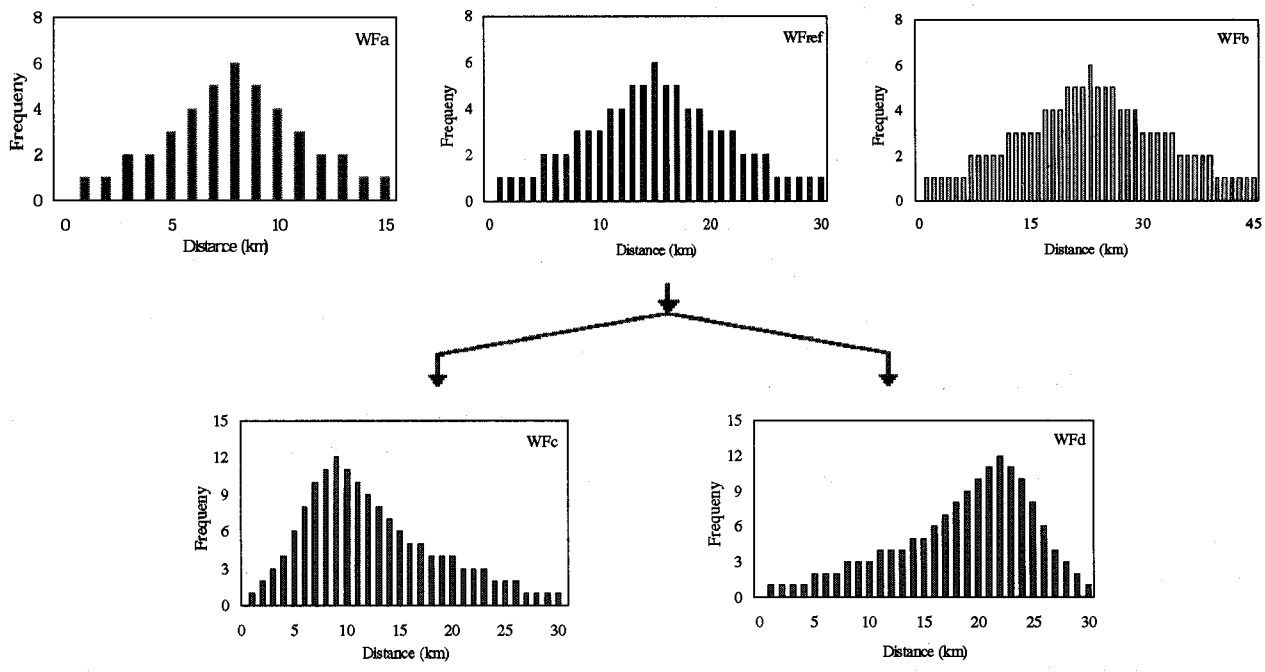

Fig. 5. *Width function shapes and base length considered in the sensitivity analysis. WF_{ref}: reference width function. WF_a and WF_b: perturbations to the base length; WF_c and WF_d: perturbations to the shape.*

(c) mean, L-coefficient of variation and L-coefficient of skewness of the soil moisture at the storm arrival time (*SAT*) and at the time of peak (*TOP*) (symbols used are m^{SM}_{SAT}, $L\text{-}CV^{SM}_{SAT}$, $L\text{-}CS^{SM}_{SAT}$, m^{SM}_{TOP}, $L\text{-}CV^{SM}_{TOP}$, $L\text{-}CS^{SM}_{TOP}$ respectively);

(d) histograms of the ratio W_o/W_m at the *SAT* and *TOP*, where W_o is current soil moisture content and W_m is soil moisture storage capacity.

The durations of 1, 6 and 12 h for the annual maximum rainfall depths were selected because the time interval 1–12 h brackets the response time of the synthetic basin considered.

The perturbations applied to the rainfall parameters are indicated in Table 3 (last row); more precisely, the same level of perturbation was applied to each parameter, independently of the month. The sensitivity of the flood frequency curve to the evapotranspiration regime was assessed by applying a perturbation of $\pm 25\%$ to the reference hourly time series as a whole and not to the individual parameters since they do not have a physical interpretation. The perturbations applied to the rainfall parameters and the potential evapotranspiration time series were selected to avoid unrealistically dry/wet soil water content regimes.

Table 4 contains the lower and the upper values of the rainfall runoff model parameters. The marked difference in the perturbation range considered for the parameters C and D is due to the structure of the convective-diffusion equation, where the celerity C is the coefficient of a first order term, while the diffusivity D is the coefficient of a second order term. Thus, a similar effect on the ffc can be anticipated if the perturbations to the two parameters differ from each other by at least one order of magnitude. Finally, the sensitivity of the ffc to the width function was assessed by considering width functions with different shapes and base lengths as shown in Fig. 5.

The results of the sensitivity analysis for the rainfall parameters are summarised by the quantities a) to d) above in Table 5, while those relevant to the sensitivity analysis of the evapotranspiration regime, rainfall-runoff model parameters and width function shapes are summarised in Table 6. Furthermore, as previously mentioned, the effect of the perturbations of each parameter on the extreme rainfall and flood frequency curves was assessed not only with the assistance of the quantities in the Tables 5 and 6 but also graphically. However, to make the qualitative analysis of the plots consistent, a framework of terms is necessary. Thus, some specific terms have been selected and used on the basis of the following considerations.

Any three parameter distribution, such as the GEV, Pareto or Generalized Logistic, can be described by a location parameter, a scale parameter and a shape parameter (Hosking and Wallis, 1997). Shape (i.e. curvature) tends to be uniquely related to L-skewness *L-CS*, but the quantile of the ffc is a function of all three parameters. If the ffc is standardised by the mean annual flood, as is the case for regional ffcs, then the quantiles will be a function of both the scale and shape parameters, and determined by *L-CV* and *L-CS* statistics. Thus, changes to the ffc observed in the graphical probability plots have been assessed by using terms such as 'upward shifting' or 'downward shifting' (although the shift may not be uniform across the full range of return period) or by 'changes in curvature'. More precisely, in the case of the unstandardised ffc, attention has been focused mainly on variation of its position/location, while, for the standardised ffc, the variation of the curvature has been the main focus.

In all the Monte Carlo experiments which have been reported here, the assumption of stationarity is implicit. The generation of rainfall, ETp and runoff time series of length 10000 years using stationary time series models represents the use of the numerical Monte Carlo method to derive the ffc, since a closed form analytical solution is not possible. Such long synthetic time series should not be regarded in the same way as observed climatic records of similar length (e.g. tree rings), which have exhibited non-stationary effects. The same stationarity assumption underlies the use of a probability distribution to describe the annual maximum discharges in a catchment as the simulation approach explored here. However, this assumption is open to question because of the possible influence of climatic change on the flood regime.

Sensitivity of rainfall and flood frequency curves to the rainfall model parameters

SENSITIVITY TO THE PARAMETER λ

The parameter λ controls the rate of storm arrival. Its inverse value represents the average time interval between storm events (inter-storm time interval). Thus, by increasing the λ value (for all the months), i.e. $\lambda+$, the average inter-storm interval decreases, while by decreasing it, i.e. $\lambda-$, the average inter-storm interval increases. As a consequence, when $\lambda \equiv \lambda+$, the climate is wetter and the average annual rainfall increases, while it decreases when $\lambda \equiv \lambda-$. Nevertheless, the perturbations to λ produce no significant effects on the rainfall frequency curves (rfc) for different durations, particularly on their curvature, as shown in Fig. 6. This observation is corroborated by the negligible variations of the values of the *L*-moments $m_{R,d}$, $L\text{-}CV_{R,d}$ and $L\text{-}CS_{R,d}$ for $d = 1,6,12$ *h*, given in Table 5. In contrast, the flood frequency curve is much more responsive to variations in λ. For $\lambda+$, the unstandardised ffc is shifted upwards, while for $\lambda-$, the opposite occurs (Fig. 7a). Moreover, the ffcs for λ, $\lambda-$ and $\lambda+$ all display a significant increase in curvature relative to the rainfall frequency curves, as reflected in the *L-CS* statistics in Table 5. When the simulated annual maximum discharges are standardised

Table 5. Summary of the results of the sensitivity analysis with respect to the rainfall model parameters.

		Ref. Set	$\lambda+$	$\lambda-$	$\nu+$	$\nu-$	$\beta+$	$\beta-$	$\alpha+$	$\alpha-$	η_1+	η_1-	η_2+	η_2-	ξ_1+	ξ_1-	ξ_2+	ξ_2-
$m_{R,1}$		13.2	13.8	12.3	12.2	14.8	13.4	13.0	13.9	12.6	11.6	15.5	13.1	13.4	11.1	17.0	12.8	14.2
$L\text{-}CV_{R,1}$		0.19	0.19	0.21	0.21	0.19	0.19	0.20	0.19	0.19	0.19	0.19	0.20	0.19	0.19	0.20	0.20	0.19
$L\text{-}CS_{R,1}$		0.24	0.23	0.24	0.25	0.24	0.24	0.24	0.25	0.23	0.24	0.24	0.24	0.24	0.23	0.25	0.25	0.23
$m_{R,6}$		26.5	28.0	24.1	23.3	31.4	27.0	25.7	25.5	27.5	24.9	29.8	23.9	30.3	24.9	29.9	23.2	32.7
$L\text{-}CV_{R,6}$		0.22	0.21	0.22	0.23	0.20	0.22	0.22	0.21	0.22	0.22	0.21	0.21	0.22	0.22	0.21	0.21	0.23
$L\text{-}CS_{R,6}$		0.28	0.27	0.27	0.29	0.26	0.28	0.28	0.28	0.28	0.29	0.26	0.27	0.28	0.29	0.26	0.26	0.30
$m_{R,12}$		31.7	33.8	28.8	27.5	38.6	32.3	31.0	30.2	33.3	30.1	35.2	27.8	38.3	30.1	35.2	27.4	39.7
$L\text{-}CV_{R,12}$		0.22	0.21	0.23	0.23	0.21	0.22	0.22	0.21	0.23	0.23	0.21	0.21	0.23	0.23	0.21	0.21	0.23
$L\text{-}CS_{R,12}$		0.29	0.29	0.29	0.30	0.27	0.29	0.30	0.29	0.29	0.31	0.27	0.28	0.31	0.31	0.27	0.27	0.31
AVP		578.0	699.1	437.9	463.2	770.8	578.0	577.9	566.4	589.4	543.0	636.2	497.3	712.4	543.0	636.1	497.3	712.4
AVE	*Value*	367.6	406.9	318.6	328.7	420.6	367.6	367.5	363.5	371.4	353.5	389.5	343.9	400.7	353.5	389.5	343.9	400.7
	%	63.6	58.2	72.7	71.0	54.6	63.6	63.6	64.2	63.0	65.1	61.2	69.2	56.2	65.1	61.2	69.2	56.2
AVSR	*Value*	85.0	126.8	47.2	52.1	164.0	85.0	84.9	81.5	88.6	74.9	104.3	59.3	141.9	74.9	104.3	59.3	142.1
	%	14.7	18.1	10.8	11.2	21.3	14.7	14.7	14.4	15.0	13.8	16.4	11.9	19.9	13.8	16.4	11.9	20.0
AVI	*Value*	125.4	165.4	72.2	82.3	186.2	125.4	125.5	121.3	129.4	114.6	142.4	94.1	169.8	114.6	142.4	94.1	169.6
	%	21.7	23.7	16.5	17.8	24.2	21.7	21.7	21.4	22.0	21.1	22.4	18.9	23.8	21.1	22.4	18.9	23.8
AVRF	*Value*	210.4	292.2	119.3	134.4	350.2	210.4	210.4	202.8	218.0	189.5	246.7	153.3	311.7	189.5	246.7	153.3	311.7
AVRC	%	36.4	41.8	27.3	29.0	45.4	36.4	36.4	35.8	37.0	34.9	38.8	30.8	43.8	34.9	38.8	30.8	43.8
m_{SAT}^{SM}		0.90	0.93	0.81	0.83	0.94	0.90	0.90	0.90	0.90	0.89	0.91	0.85	0.93	0.89	0.91	0.85	0.93
$L\text{-}CV_{SAT}^{SM}$		0.06	0.04	0.11	0.10	0.04	0.06	0.06	0.06	0.07	0.07	0.06	0.09	0.05	0.07	0.06	0.09	0.05
$L\text{-}CS_{SAT}^{SM}$		−0.46	−0.49	−0.36	−0.39	−0.49	−0.46	−0.45	−0.45	−0.46	−0.44	−0.47	−0.39	−0.51	−0.45	−0.47	−0.39	−0.51
m_{TOP}^{SM}		0.96	0.99	0.89	0.91	1.00	0.96	0.96	0.96	0.97	0.95	0.98	0.92	0.99	0.95	0.98	0.92	0.99
$L\text{-}CV_{TOP}^{SM}$		0.03	0.01	0.07	0.06	0.00	0.03	0.03	0.03	0.03	0.04	0.02	0.05	0.01	0.04	0.02	0.06	0.01
$L\text{-}CS_{TOP}^{SM}$		−0.64	−0.86	−0.33	−0.37	−0.94	−0.64	−0.64	−0.61	−0.67	−0.56	−0.77	−0.41	−0.91	−0.56	−0.76	−0.40	−0.92
m_Q		21.7	32.2	11.4	11.5	42.5	22.0	21.3	20.1	23.7	18.5	28.6	12.7	40.0	18.5	28.6	12.5	41.6
$L\text{-}CV_Q$		0.39	0.34	0.41	0.40	0.30	0.39	0.39	0.38	0.41	0.40	0.37	0.40	0.33	0.40	0.37	0.39	0.34
$L\text{-}CS_Q$		0.37	0.32	0.50	0.50	0.29	0.36	0.37	0.35	0.38	0.41	0.32	0.47	0.33	0.41	0.32	0.47	0.33

Table 6. Summary of the results of the sensitivity analysis with respect to the rainfall-runoff model parameters and potential evapotranspiration demand.

		Ref. Set	W_m+	W_m-	$b+$	$b-$	d_1+	d_1-	d_2+	d_2-	$C+$	$C-$	$D+$	$D-$	*WFa*	*WFb*	*WFc*	*WFd*	*WFe*	$ETp+$	$ETp-$
AVE	*Value*	367.6	401.3	323.9	347.4	374.6	363.2	374.4	373.9	348.2	367.6	367.6	367.6	367.6	367.6	367.6	367.6	367.6	367.6	411.9	283.7
	%	63.6	69.4	56.0	60.1	64.8	62.8	64.8	64.7	60.3	63.6	63.6	63.6	63.6	63.6	63.6	63.6	63.6	63.6	71.3	49.1
AVSR	*Value*	85.0	72.3	130.8	147.7	61.5	74.5	111.8	94.2	69.4	85.0	85.0	85.0	85.0	85.0	85.0	85.0	85.0	85.0	69.3	114.4
	%	14.7	12.5	22.6	25.6	10.6	12.9	19.3	16.3	12.0	14.7	14.7	14.7	14.7	14.7	14.7	14.7	14.7	14.7	12.0	19.8
AVI	*Value*	125.4	104.3	123.2	82.9	141.8	140.3	91.8	109.8	160.4	125.4	125.4	125.4	125.4	125.4	125.4	125.4	125.4	125.4	96.8	179.8
	%	21.7	18.0	21.3	14.3	24.5	24.3	15.9	19.0	27.7	21.7	21.7	21.7	21.7	21.7	21.7	21.7	21.7	21.7	16.8	31.1
AVRF	*Value*	210.4	176.6	254.1	230.6	203.3	214.8	203.6	204.1	229.7	210.4	210.4	210.4	210.4	210.4	210.4	210.4	210.4	210.4	166.1	294.2
AVRC	%	36.4	30.6	44.0	39.9	35.2	37.2	35.2	35.3	39.7	36.4	36.4	36.4	36.4	36.4	36.4	36.4	36.4	36.4	28.7	50.9
m_{SAT}^{SM}		0.90	0.83	0.85	0.78	0.94	0.86	0.95	0.93	0.83	0.89	0.91	0.90	0.90	0.89	0.90	0.90	0.90	0.90	0.88	0.92
$L\text{-}CV_{SAT}^{SM}$		0.06	0.09	0.11	0.12	0.04	0.08	0.04	0.05	0.10	0.07	0.05	0.07	0.07	0.07	0.06	0.06	0.07	0.06	0.08	0.05
$L\text{-}CS_{SAT}^{SM}$		−0.46	−0.35	−0.41	−0.34	−0.48	−0.38	−0.60	−0.52	−0.31	−0.46	−0.45	−0.46	−0.46	−0.46	−0.46	−0.45	−0.46	−0.45	−0.45	−0.41
m_{TOP}^{SM}		0.96	0.89	1.00	0.87	0.99	0.94	0.99	0.98	0.91	0.96	0.97	0.96	0.96	0.96	0.96	0.97	0.96	0.97	0.94	0.99
$L\text{-}CV_{TOP}^{SM}$		0.03	0.07	0.00	0.07	0.01	0.04	0.01	0.02	0.06	0.03	0.02	0.03	0.03	0.03	0.03	0.03	0.03	0.03	0.04	0.01
$L\text{-}CS_{TOP}^{SM}$		−0.64	−0.33	−0.81	−0.31	−0.84	−0.43	−0.90	−0.79	−0.34	−0.64	−0.64	−0.65	−0.64	−0.64	−0.64	−0.64	−0.65	−0.64	−0.53	−0.80
m_Q		21.7	11.9	45.1	21.5	24.2	17.9	28.6	24.8	16.3	30.6	11.5	21.7	22.4	33.0	21.7	16.4	25.0	20.3	17.1	31.5
$L\text{-}CV_Q$		0.39	0.35	0.30	0.27	0.39	0.41	0.31	0.36	0.43	0.40	0.37	0.39	0.39	0.40	0.39	0.38	0.40	0.39	0.41	0.37
$L\text{-}CS_Q$		0.37	0.48	0.34	0.39	0.29	0.48	0.26	0.31	0.50	0.37	0.34	0.36	0.37	0.37	0.37	0.36	0.37	0.37	0.41	0.35

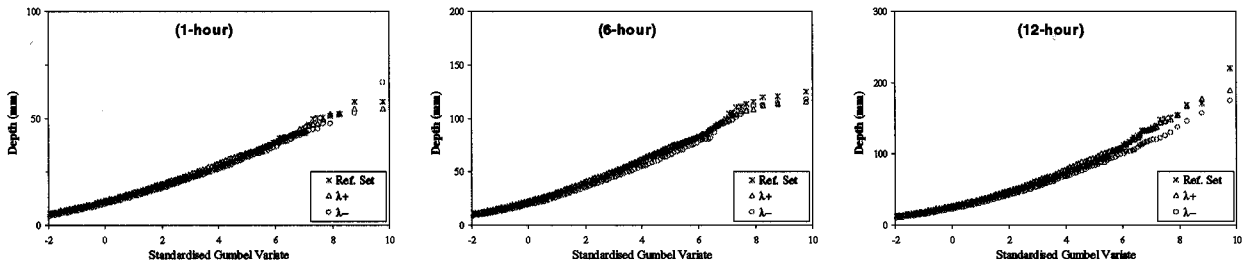

Fig. 6. *Sensitivity analysis of parameter λ. Frequency curves for the annual maximum rainfall depths for durations of 1, 6 and 12 h.*

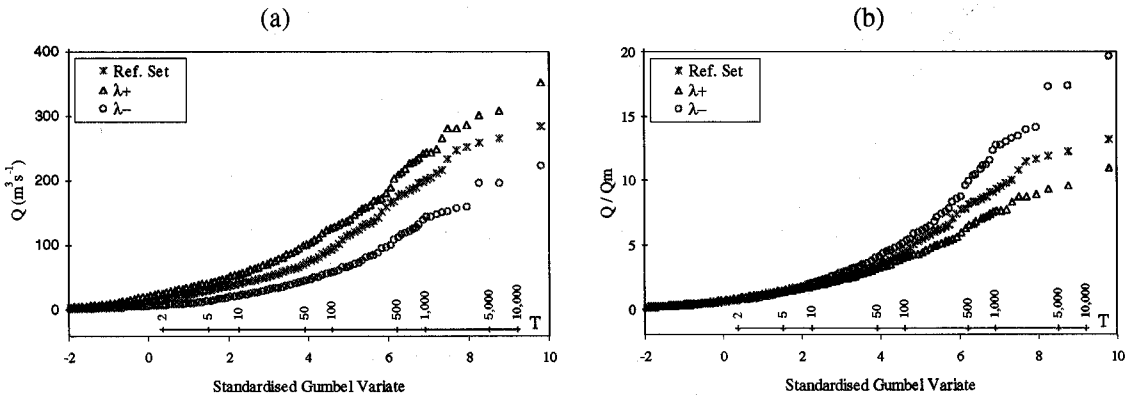

Fig. 7. *Sensitivity analysis of parameter λ. Flood frequency curves in (a) unstandardised and (b) standardised forms.*

by the mean annual flood m_Q, the positions of the ffcs corresponding to $\lambda+$ and $\lambda-$ are reversed (Fig. 7b), due to the fact that the $\lambda-$ ffc has greater curvature and higher *L-CS* than the λ and $\lambda+$ ffcs (Table 5).

The reason for this behaviour has been investigated and it has been found that the soil moisture regime exercises a strong control on the ffc. A lower value of λ corresponds to a drier climate which implies larger and more extended soil moisture deficits. Thus, the probability that a storm event occurs when the soil is wet becomes smaller. On the contrary, when λ increases, the soil does not have the opportunity to dry out between the storm events and so the probability that a storm event occurs when the soil is wet becomes larger. The frequency distributions of the standardised soil moisture (W_o/W_m) at the storm arrival time (*SAT*) and time of peak (*TOP*) (Fig. 8) and their moments (Table 5) corroborate these observations. Figure 8 shows, for example, that when $\lambda \equiv \lambda+$, the soil moisture content is more than 90% of the soil moisture storage capacity with a frequency of 80% at *SAT* and 95% at *TOP*, while, when $\lambda \equiv \lambda-$, the soil moisture content is more than 90% of the soil moisture storage capacity with remarkably smaller frequencies i.e. about 38% at *SAT* and about 60% at *TOP*.

The previous comments can be summarised as follows. When the perturbation of the parameter λ produces, at the characteristic times *SAT* and *TOP*, a distribution of the soil moisture content concentrated close to saturation, the

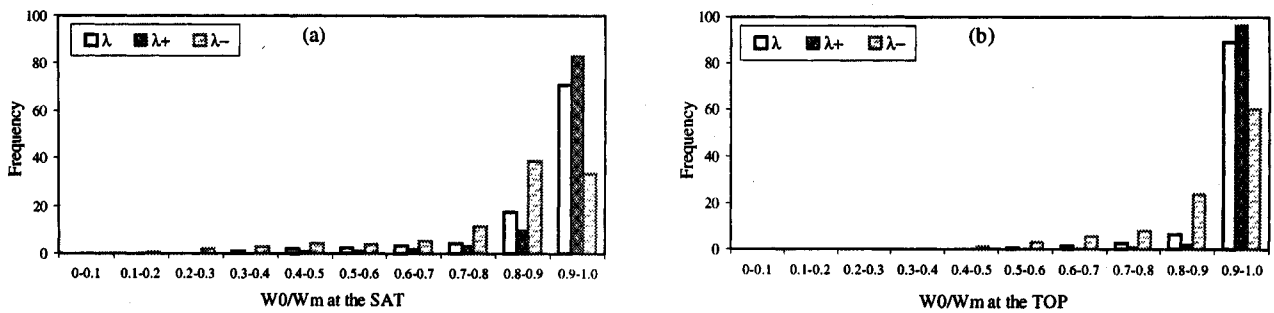

Fig. 8. *Sensitivity analysis of parameter λ. Frequency histogram of the standardised soil moisture content W_o/W_m at (a) the storm arrival time (SAT) and (b) time of peak (TOP).*

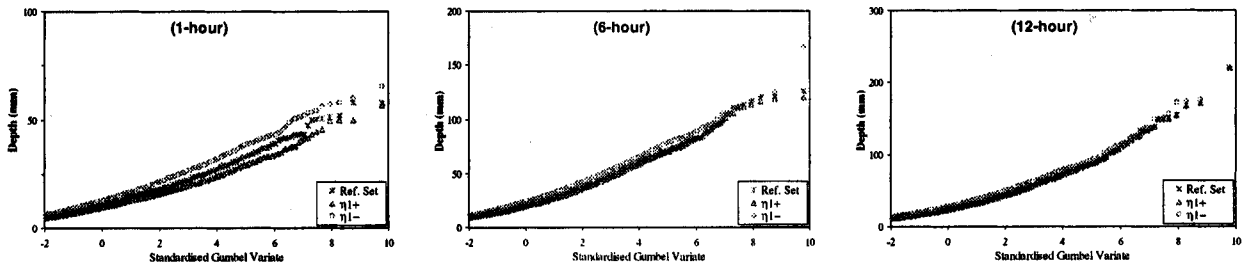

Fig. 9. *Sensitivity analysis of parameter η_1. Frequency curves for the annual maximum rainfall depths for durations of 1, 6 and 12 h.*

unstandardised flood frequency curve tends to move upwards while its curvature tends to decrease. On the contrary, when the perturbation produces, at the characteristic times, a distribution of the soil moisture content with lower mean, higher dispersion and smaller negative skewness (i.e. a longer tail), the unstandardised flood frequency curve shifts downwards and its curvature increases. When standardised, the curves reverse their positions, reflecting their respective curvatures.

The sensitivity of the annual water balance to perturbations in λ has also been analysed, and annual average rainfall *AVP* has been decomposed into actual evapotranspiration (*AVE*), surface runoff (*AVSR*), and interflow (*AVI*) expressed as percentages; total runoff (*AVRF*) is the sum of *AVSR* and *AVI* (Table 5). As expected, *AVP* responds to perturbations in λ; for $\lambda+$, the percentages of *AVSR*, *AVI* and *AVRF* increase, and the percentage of *AVE* decreases, while, for $\lambda-$, the opposite occurs. These results are all physically consistent with the observations made above on the soil moisture regimes for $\lambda+$ and $\lambda-$.

In summary, the unstandardised ffc for $\lambda-$is below that for $\lambda+$, the corresponding m_Q is smaller but $L\text{-}CS_Q$ is larger which implies a larger upward curvature and thus the standardised ffc for $\lambda-$is above that for $\lambda+$.

SENSITIVITY TO THE PARAMETERS ν, η_1, η_2, ξ_1, ξ_2

These parameters control the number of rain cells (parameter ν), heavy and light cell durations (parameters η_1, η_2) and intensities (parameters ξ_1, ξ_2). The inverse of each of them is the average value of the corresponding random variate. So, the inverse of η_1, i.e. η_1^{-1} is the average duration of the heavy cells within a storm. As a consequence, by decreasing its value, the average duration increases and, on average, more rainfall is generated by this type of cell, all the other parameters remaining constant. This produces an increase in total annual rainfall as shown by the value *AVP* in Table 5. Furthermore, an increase in the annual maximum rainfall depths of given return period is observed mainly for a duration of 1 hour (Fig. 9). Indeed, this parameter is related to the heavy cells which represent the convective storm events. The same considerations apply to the parameter ξ_1.

Perturbations to the two parameters η_2 and ξ_2 have the same effect on *AVP* and on the rainfall frequency curves. However, their effect is particularly evident in the position of the rainfall frequency curve for the longer durations (Fig. 10) and this is coherent with the fact that these two parameters represent the light cells. i.e. the cyclonic rainfall events. Finally, for the parameter ν, one can observe that its increment (decrement) produces a significant decrement (increment) of $m_{R,d}$ but little variation in $L\text{-}CV_{R,d}$ and $L\text{-}CS_{R,d}$ (Table 5). This means that, more than in the previous cases for the other four parameters, the probability distribution of the annual maximum rainfall for different durations is simply shifted up/down without changing its curvature.

To summarise, the alterations to the rainfall regime produced by the perturbations to the five parameters ν, η_1, η_2, ξ_1, ξ_2 are consistent with the results observed for perturbations to the parameter λ (Note: a positive increment in one of these parameters produces a similar effect to a negative increment in λ because of the parameter defini-

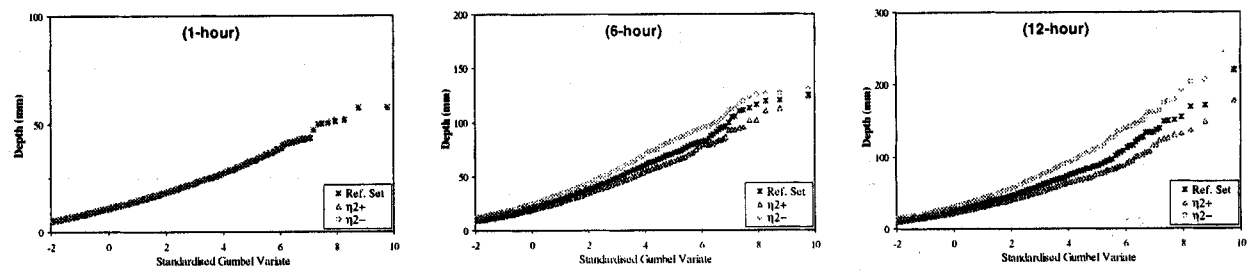

Fig. 10. *Sensitivity analysis of parameter η_2. Frequency curves for the annual maximum rainfall depths for durations of 1, 6 and 12 h.*

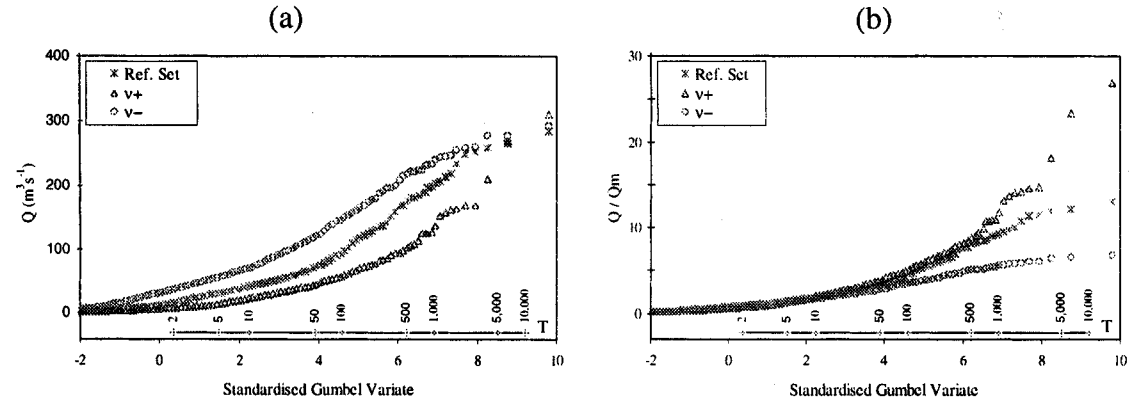

Fig. 11. *Sensitivity analysis of parameter v. Flood frequency curves in (a) unstandardised and (b) standardised forms.*

tions). Therefore, on the basis of the considerations developed for λ, an increment (decrement) of these five parameters is expected to produce similar effects on the probability distribution of the soil moisture content at the *SAT* and, thus, the same effect on the ffc. This is confirmed by Fig. 11 where, as an example, it is possible to observe that the curvature of the standardised flood frequency curve increases when v increases, while the unstandardised flood frequency curve moves down.

SENSITIVITY TO THE PARAMETERS α, β

The parameters α and β control the percentage of the heavy cells in a storm and the displacement of the rain cells relative to the storm origin, respectively. The parameter α is dimensionless and its increment/decrement implies directly an increment/decrement of the proportion of the heavy cells per storm. The inverse of β, i.e. β^{-1}, is the average value of the displacement time of the rain cells after the storm origin. Perturbations to these two parameters apparently have no effect either on the rainfall or flood frequency curves. Table 5 shows that the perturbations do not result in significant changes either to *AVP* and the other annual average values (*AVI*, *AVSR*, *AVE*), or to the statistics of the annual maximum rainfall depths. Of course, no significant changes in the rainfall and flow regimes indicate that no significant change occurs in the soil moisture regime, and thus both the standardised and unstandardised ffcs remain unchanged. These considerations are corroborated also by the fact that all the *L-moment* statistics, both for rainfall and discharge, remain unchanged (Table 5).

Sensitivity to the potential evapotranspiration

Potential evapotranspiration represents a climatic factor that, like the rainfall regime, is expected to have an important influence on the soil moisture regime, and therefore on the ffc, since an increase in *ETp* tends to enhance the depletion of the soil moisture. Thus, more extended soil moisture deficits are produced and the probability that a storm event occurs when the soil is wet becomes smaller and smaller and so the dry soil produces a strong damping effect on the peak floods, notably for lower return periods. A decrease in the potential evapotranspriation rate produces the opposite effect.

These considerations highlight a marked analogy with the effect of the parameter λ of the rainfall model, since the potential evapotranspiration rate directly affects the intensity and duration of the dry and wet soil moisture spells. These considerations are confirmed by the sensitivity analysis, the results of which can be interpreted as for those of the parameter λ. In particular, Fig. 12 shows the unstandardised and standardised ffcs where an increase in the curvature is observed for ETp+, while the corresponding variations of the statistics m_Q, $L\text{-}CV_Q$ and $L\text{-}CS_Q$ can be observed in Table 6 (similar behaviour is observed when $\lambda \equiv \lambda-$).

Moreover, Fig. 13 shows that when $ETp = ETp+$, the soil moisture content is more than 90% of the soil moisture storage capacity with a low frequency of about 60% at *SAT* and 80% at *TOP*, while, when $ETp = ETp-$, the soil moisture content is more than 90% of the soil moisture storage capacity with a higher frequency of about 80% at the storm arrival time and 95% at the time of peak. The way in which this alteration of the soil moisture regime is reflected in the ffcs has already been explained for the parameter λ.

A preliminary conclusion can be drawn from the discussion presented above with reference to the climatic factors (i.e. rainfall and potential evapotranspiration). It has been shown that these factors affect the ffc by altering the soil moisture regime. In particular, when the perturbation of the parameter considered produces, at the *SAT*, distributions of the soil moisture concentrated close to saturation, the unstandardised ffc tends to move upwards while its curvature tends to decrease. The contrary applies when the perturbation produces, at the *SAT*, distributions of the soil

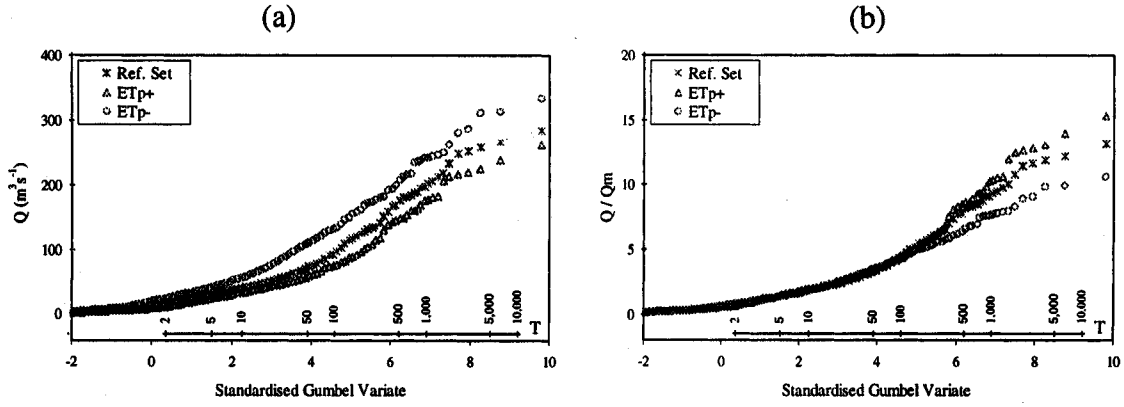

Fig. 12. *Sensitivity analysis of potential evapotranspiration demand. Flood frequency curves in (a) unstandardised and (b) standardised forms.*

moisture content with lower mean, higher dispersion and smaller negative skewness. This systematic behaviour suggests that the soil moisture content probability distribution at the *SAT* might be considered as the *link between the perturbations to the individual parameters and their effects on the ffc*. This latter statement will be supported also by the sensitivity analysis of all the rainfall runoff model parameters, as shown below.

Sensitivity of the flood frequency curve to the rainfall-runoff model parameters

As already noted, the rainfall runoff model has six parameters. Four of them (W_m, b, d_1 and d_2) are relevant to the water balance component, while the remaining two (C and D) are relevant to the channel routing component. The width function is also included in the sensitivity analysis.

The parameters d_1 and d_2 control the interflow component which affects the rate of soil moisture depletion. Thus, a clear analogy can be defined with the analysis already conducted for the climate parameters. For continuity with the previous section, the results of the sensitivity analysis for the parameters d_1 and d_2 are analysed first.

This decision also reflects an awareness of the interaction existing between the parameters W_m and b, as shown by Eqn. (3), which makes them interdependent. As a consequence, when one of them is altered and the other is maintained constant, an indirect perturbation is also applied to the value of the maximum point storage capacity w_{max}, i.e. two characteristics of the soil are altered at the same time. This makes it impossible to perform correctly the sensitivity analysis based on the *one-at-a-time* parameter perturbation, as done for all the other parameters.

Nevertheless, this type of analysis was also performed for W_m and b because it provides some insight into the effects of the soil storage capacity on the flood frequency curve. Further consideration of the fact that the results obtained for one perturbed parameter may be influenced by the level of the unperturbed parameter (b or W_m) will be discussed in the conclusions and in Franchini *et al.* (2000).

SENSITIVITY TO THE PARAMETERS d_1 AND d_2

These two parameters control the interflow/drainage rate. In particular, d_1 represents the maximum interflow rate that occurs when the soil is completely saturated. As a consequence, its increment/decrement has a direct effect

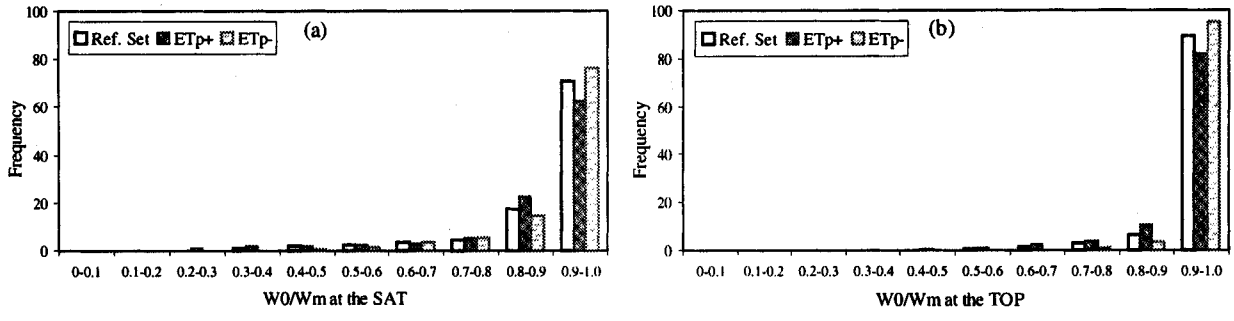

Fig. 13. *Sensitivity analysis of potential evapotranspiration demand. Frequency histogram of the standardised soil moisture content W_o/W_m at (a) the storm arrival time (SAT) and (b) time of peak (TOP).*

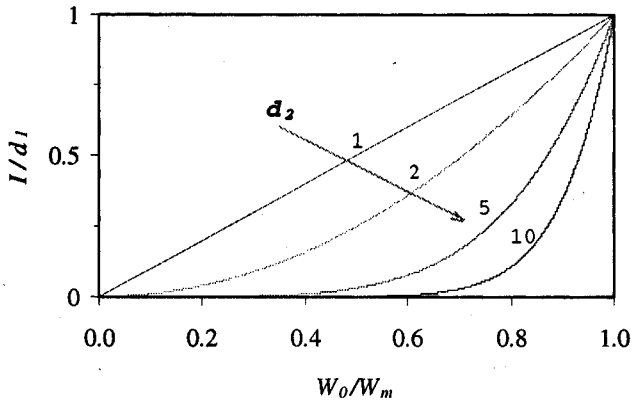

Fig. 14. *Sensitivity analysis of parameter d_2. Effect of this parameter on the shape of the interflow equation.*

on this flow component. The parameter d_2 controls the shape of the relationship between the soil moisture content and the interflow as shown in Fig. 14 where it is clear that an increment of d_2 produces a larger upward curvature and so less water is released from the soil for a given soil moisture content. Consequently, an increment of the parameter d_1 and a decrement of the parameter d_2 both produce an increment of the interflow rate for a given soil moisture content, which tends to enhance the depletion of the soil moisture. Therefore, more extended soil moisture deficit regimes are expected and the probability that a storm event occurs when the soil is wet becomes smaller and smaller. Similarly, a decrement of the interflow rate produces the opposite situation.

It is now clear that the same considerations previously discussed with reference to the rainfall model parameters, e.g. λ, can be applied also to this case. In fact, the parameter λ and the two parameters d_1 and d_2 directly affect the intensities and durations of the dry and wet soil moisture spells, but through different mechanisms. These qualitative considerations are confirmed by the quantitative results of the sensitivity analysis, some examples of which are discussed below. Figure 15 clearly shows that the curvature of the ffc increases when the interflow is increased (i.e. when $d_1 \equiv d_1+$, or $d_2 \equiv d_2-$) and the corresponding variations of the statistics m_Q, $L\text{-}CV_Q$ and $L\text{-}CS_Q$ can be observed in Table 6. Figure 16 shows that when $d_1 \equiv d_1+$ the soil moisture content is more than 90% of the soil moisture storage capacity with a low frequency of about 50% at *SAT* and 80% at *TOP*, while, when $d_1 \equiv d_1-$, the soil moisture content is more than 90% of the soil moisture storage capacity with a frequency of 90% at *SAT* and 98% at *TOP*. These alterations of the soil moisture regime are reflected in the flood frequency curves through the mechanism already discussed for the parameter λ.

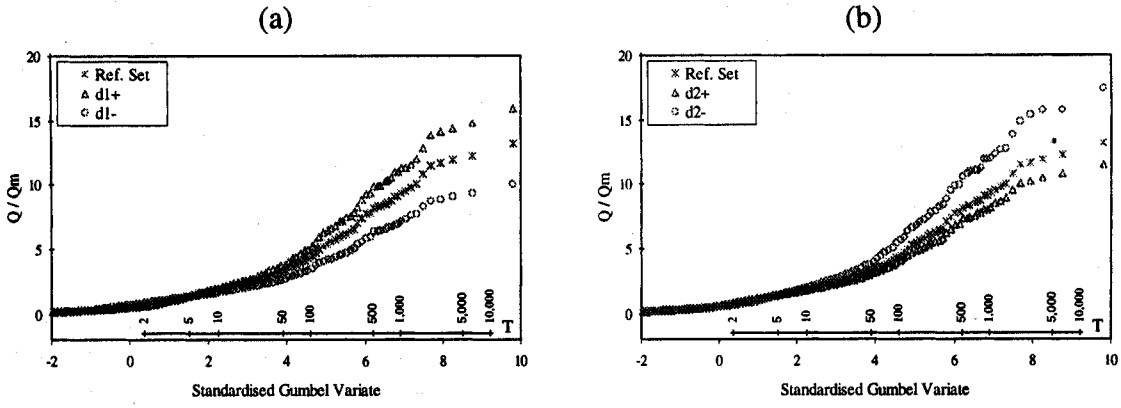

Fig. 15. *Sensitivity analysis of parameters d_1 and d_2. Flood frequency curves in standardised forms.*

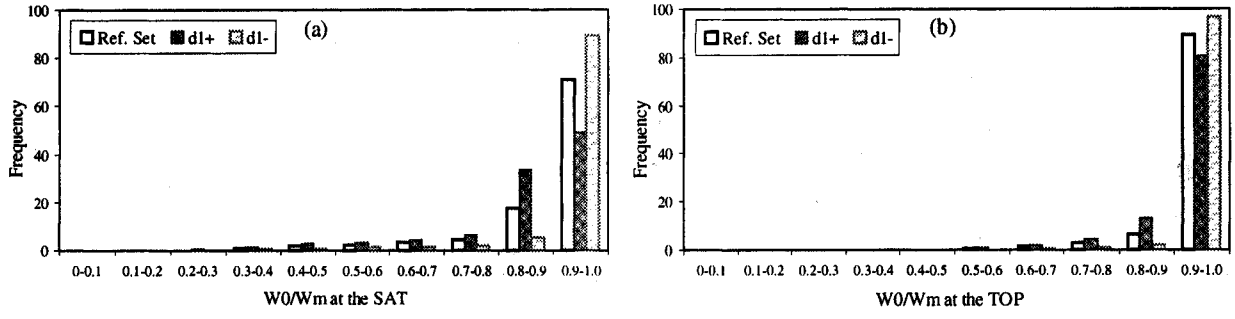

Fig. 16. *Sensitivity analysis of parameter d_1. Frequency histogram of the standardised soil moisture content W_o/W_m at (a) the storm arrival time (SAT) and (b) time of peak (TOP).*

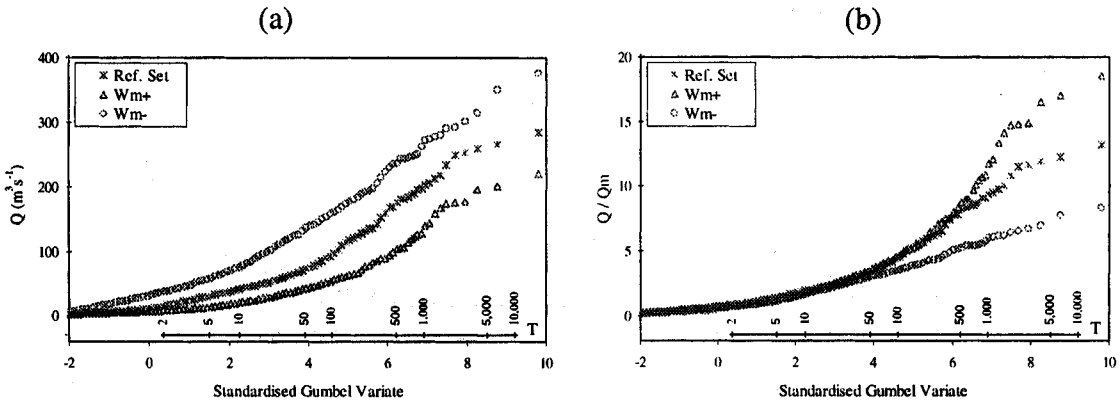

Fig. 17. *Sensitivity analysis of parameter W_m. Flood frequency curves in (a) unstandardised and (b) standardised forms.*

SENSITIVITY TO THE PARAMETER W_M

In the framework of the rainfall runoff model used here, W_m represents the average value of the point soil moisture storage capacity in the basin. The other 'storage' information is given by the parameter w_{max}, which is the maximum point soil moisture storage capacity. The point storage capacity is not assumed constant over the basin and its probability distribution is qualitatively represented in Fig. 2. Obviously, a value of W_m equal to zero (and, as a consequence, $w_{max} = W_m\ (b+1) = 0$ [see Eqn. 3]) means a completely impervious soil without storage capacity. In such a case, the frequency distribution of the flood peaks is expected to be identical to that of the rainfalls which produce them because of the lack of any intermediate damping action from the soil. On the contrary, the bigger the soil storage capacity W_m, the bigger the damping effect, and the amount of precipitation during a storm event can only rarely reach and exceed the soil capacity. This implies that the difference between the ffc and the corresponding curves of the annual maximum rainfall depths for different durations tends to increase and, at the same time, the situation where the whole basin contributes to the runoff (which occurs only when w_{max} is exceeded) becomes more rare. Thus, a larger curvature of the flood frequency curve is expected as the soil storage capacity tends to increase. Of course, a larger soil storage capacity, due to its higher damping action, is also expected to reduce the value of the annual flood peak for any given return period.

These intuitive considerations are confirmed by the results of the sensitivity analysis. Figure 17 shows clearly that, when W_m increases, the discharge for a given return period becomes smaller but the difference between the less extreme and more extreme events becomes bigger (Fig. 17b) and the L-skewness coefficient $L\text{-}CS_Q$ increases (see Table 6).

Alterations to the values of *AVE*, *AVSR*, *AVI* and *AVRC* are also worthy of comment. The annual average rainfall amount *AVP* remains constant but its subdivision into the three components *AVE*, *ASR* and *AVI* changes. In particular, when $W_m \equiv W_m-$the surface runoff component increases. This can be easily explained by observing that a reduction of the soil moisture storage capacity implies that less rainfall infiltrates into the soil. On the other hand, due to the fact that less water enters the soil, the magnitude of the actual evapotranspiration within the annual water balance is reduced.

SENSITIVITY TO THE PARAMETER b

The parameter b controls the shape of the probability distribution of the point soil moisture storage capacity, as shown by Eqn. (2) where it is also evident that, for a given value of W_m, b controls the dynamics of the area contributing to surface runoff. Therefore, it might be expected that a perturbation to b would produce an impact on the ffc, but Fig. 18 demonstrates that no clear impact is evident. However, the strong interaction between b and W_m, through Eqn. (3) has already been noted, and this apparent lack of sensitivity to b may well be a function of the reference value of W_m. Therefore, in this particular case, the *one-at-a-time* perturbation analysis can only offer limited information on the effects of both parameters which might even be misleading. As a consequence, a different approach based on a full experimental design technique, which takes account of parameter interactions, is necessary, and this is the focus of Part II which also reveals the presence of many other parameter interactions and their effects on the ffc.

SENSITIVITY TO THE PARAMETERS C AND D

Once the width function characterising the channel network has been defined, the parameters C and D control the hydraulic aspects of the routing component of the rainfall runoff model. The effect of these two parameters on the flood frequency curve is shown in Fig. 19.

Figure 19a relates to the parameter C: an increase and a decrease in the discharge value for a given return period is observed for $C \equiv C+$ and $C \equiv C-$, respectively, or, in

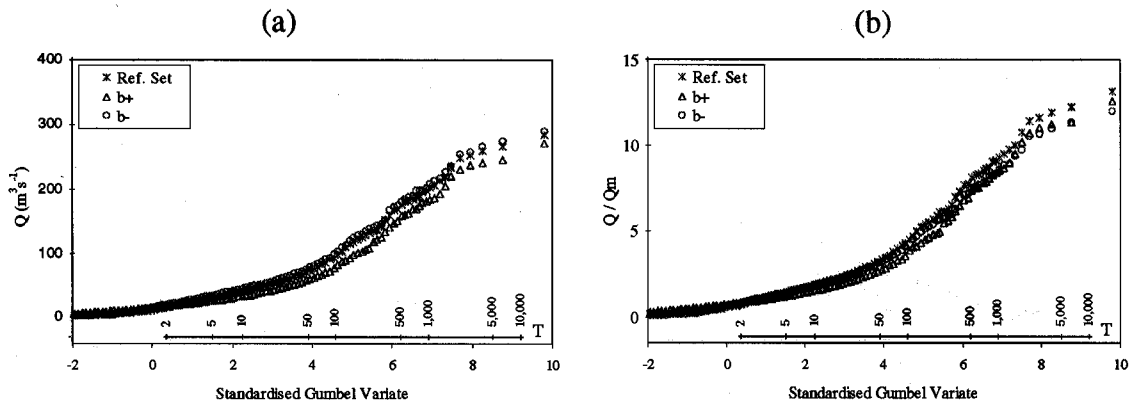

Fig. 18. *Sensitivity analysis of parameter b. Flood frequency curves in (a) unstandardised and (b) standardised forms.*

other words, the unstandardised ffc shifts upward when $C \equiv C+$, and downwards when $C \equiv C-$. Similar results, but in the reverse order, are observed when the parameter D is perturbed (Fig. 19c).

On the other hand, Figs. 19b and 19d show that, when the ffcs are standardised, they collapse onto each other. This implies that the parameters of the linear routing component do not control the curvature of the ffc, even if the discharge values for different return periods can be altered.

As regards the effect on the unstandardised ffc, this can be explained easily from a hydraulic point of view. An increment of the celerity, with the diffusivity D held constant, tends to sharpen the flood wave and thus the flood peaks tend to be higher. The opposite applies when the

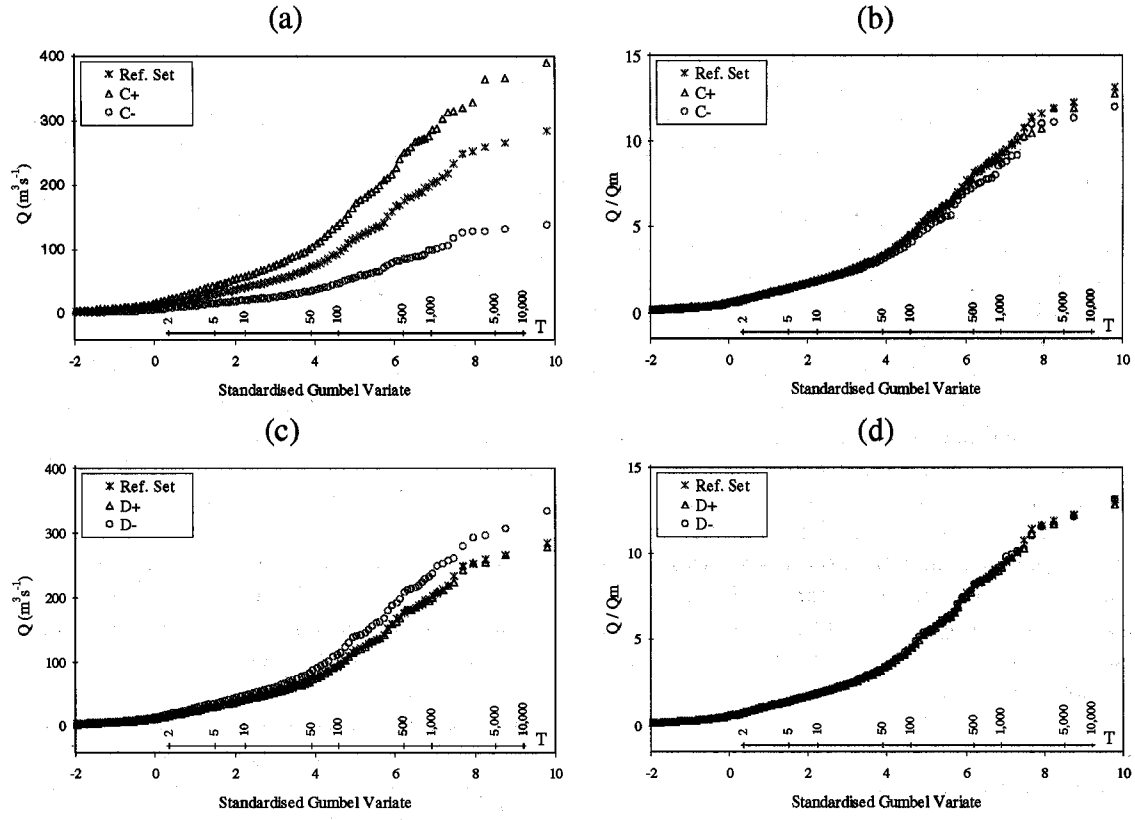

Fig. 19. *Sensitivity analysis of parameters C and D. Flood frequency curves in unstandardised (a, c) and standardised forms (b, d).*

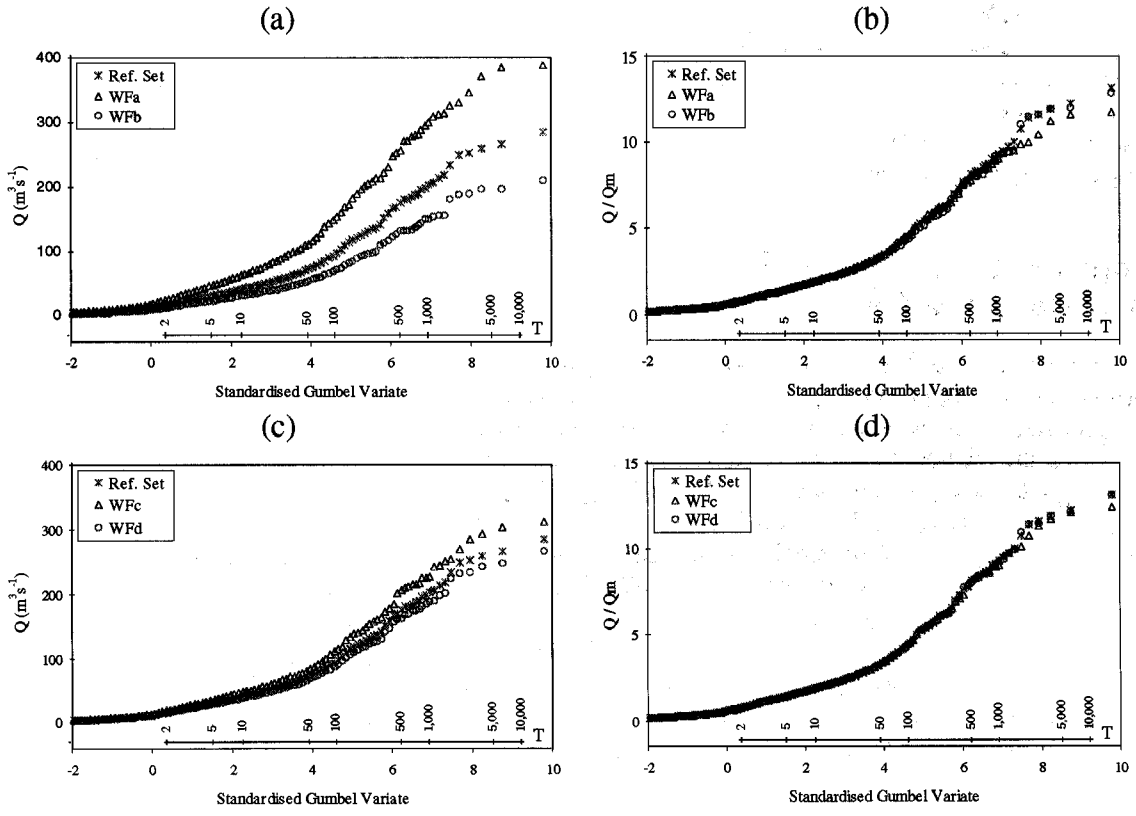

Fig. 20. *Sensitivity analysis of the width function shape and base length. Flood frequency curves in unstandardised (a, – WFa,b; c – WFc,d) and standardised forms (b – WFa,b; d – WFc,d).*

celerity is reduced. Similar results, but in reverse order, apply when the parameter D is perturbed.

However, it is important to realise that this result is strictly related to the structure of the routing component of the rainfall runoff model where the downstream propagation is represented through a *lumped, linear* formulation. Indeed, this type of formulation makes it impossible to simulate, for example, the interaction between the main channel and the flood plain or inundated valley, which, as it is well known, can have a heavy impact on the flood celerity and attenuation. Also natural or man-made storage capacities, or other man-made devices that modify the flood wave above a certain discharge value, are not represented by the routing component. On the other hand, all these latter aspects produce, in the real world, a storage effect that could exert a similar action to that exerted by the soil moisture storage capacity, thus affecting both the unstandardised and standardised ffcs. However, these storage effects are not represented by the routing component of the rainfall runoff model and thus their influence on the ffc cannot be detected by the sensitivity analysis.

SENSITIVITY TO THE WIDTH FUNCTION

The results for the perturbations applied to the reference width function *WFref* are shown in Fig. 20. A first perturbation is performed by reducing (*WFa*) or increasing (*WFb*) the length of the channel network, while keeping the shape of *WF* constant (i.e. symmetric) (Fig. 5). The second perturbation is performed by imposing a positive (*WFc*) or negative (*WFd*) skewness on the *WF*, while keeping the base length constant. In all these cases, the area of the basin is kept constant and equal to 100 km^2.

Figure 20a shows that an increment of the discharge value for a given return period is observed when the base length is reduced (*WFa*) and a decrement when it is increased (*WFb*). In fact, *WFb* is related to an elongated basin, thus producing a larger attenuation of the flood wave. Also, in the case in which the width function shape is perturbed (Fig. 20c), an increment of the discharge value for a given return period is observed for the *WFc* (positive skewness) while a decrement is observed for the *WFd* (negative skewness). The explanation of this behaviour is similar to that used for the cases of *WFa* and *WFb*. The positive skewness of *WFc* implies a decrement of the length of the average travel path that a droplet has to follow to reach the basin outlet. Thus, a smaller attenuation effect is performed by the channel network and the discharge value for a given return period tends to increase. The opposite applies for the case of *WFd*.

In conclusion, a similar statement can be made about

perturbations to the *WF* as to the parameters *C* and *D*, i.e. they do not alter the curvature of the unstandardised ffc curve but only its location by producing an upward/downward shift. However, it is worth noting that this conclusion relates strictly to the lumped-linear formulation of the routing component of the rainfall runoff model used.

Some comments on the physical realism of the model simulations

The overall sensitivity analysis has been performed using models which incorporate several simplifying assumptions. Nevertheless, they reflect well defined physical characteristics, particularly for the rainfall and basin soil characteristics, and thus the results have quite a general validity from a conceptual point of view. However, the statistics shown in Tables 5 and 6, relevant to annual quantities such as the annual average precipitation (*AVP*) or the runoff coefficient (*AVRC*) *etc.* reveal that the 'range' of the climate analysed in the current study may be typical of a **relatively humid region**, but at the dry end of the humid scale, with runoff coefficient varying between 0.3 and 0.5. In Franchini *et al.* (2000), as already noted, a wider range of climatic and basin conditions is analysed.

Nonetheless, it is worth stressing that all the previously mentioned values of the water balance at basin level (Tables 5 and 6) are coherent with those observed, for example, in the South East of England. Indeed, all the simulations performed in this sensitivity analysis can be considered representative of **surface water basins**, i.e. basins where the flow at the outlet is mainly due to interflow and surface runoff components.

The influence of groundwater has not been investigated here since this component was excluded from the rainfall runoff model to limit the number of parameters to be treated. It is expected that its influence leads to a heavy damping effect on the flood response, thus producing smaller values of the statistics of the annual maxim flood, such as m_Q and $L\text{-}CV_Q$. However, the overall effect on the unstandardised and standardised ffcs is not known and needs to be investigated in a future study.

Discussion and conclusions

The experiments described above show that climatic factors, represented by the rainfall and potential evapotranspiration regimes, and basin soil characteristics can exert strong influences on the properties of the ffc. The climatic factors mainly affect the ffc by altering the soil moisture regime. For example, perturbations to the storm arrival time rate (parameter λ), the number of cells per storm (parameter v), the duration and the intensity of the rain cells (parameters η_i and ξ_i) clearly alter the water balance (see Table 5), and *the probability distribution of the soil moisture at the storm arrival time*, as shown through several examples in the previous analysis. In particular, when the perturbation of the parameter considered produces, at the characteristic times *SAT* and *TOP*, distributions of the soil moisture concentrated close to saturation, the unstandardised ffc tends to move upwards while its curvature tends to decrease. On the contrary, when the perturbation produces, at the characteristic times, distributions of the soil moisture content with lower mean, higher dispersion and smaller negative skewness (i.e. a longer tail), the unstandardised ffc shifts downwards and its curvature increases. When standardised, the curves reverse their positions reflecting their respective curvatures.

However, not all the rainfall model parameters have a significant effect on the ffc; the displacement of the rain cells in a storm (parameter β) and the proportion of the heavy cell type (parameter α) do not affect significantly even the average behaviour of the rainfall time series.

The drainage properties of the soil (parameters d_1 and d_2) exert their effect on the ffc through the same soil moisture mechanism discussed above. In fact, when a perturbation produces an increment in the interflow rate, the depletion of the soil moisture is accelerated, thus affecting the probability distribution of the soil moisture at the storm arrival time.

The local soil moisture storage capacity and its distribution are controlled by the parameters W_m and b, respectively, and their combination mainly affects the ffc through the combination of the damping effect of the soil storage capacity and the dynamic variation of the area contributing to surface runoff during a storm event.

It will be recalled that these two parameters are inversely related to each other within the model, and the effect on the ffc of a perturbation to one of them depends on the reference value given to the other. This implies that the sensitivity analysis based on *one-at-a-time* perturbation analysis is inappropriate for studying their effects. Nevertheless, within this type of analysis some intuitively appealing behaviour for the parameter W_m was observed, while the results for the parameter b might suggest that it has a limited influence on the ffc. However, these results are a consequence of the reference level of the parameter W_m used in this study; several other tests performed with different value of W_m and b, not presented here, have produced, in some cases, reverse results and, in particular, showed that, when the effect of one of the two parameters was clear and readily interpretable, the effect of the other always appeared to be negligible or difficult to understand. This requires the application of a formal experimental design technique to highlight both the main effect of each of the parameters and their interactions, on the unstandardised and standardised ffcs; this more complex approach is discussed in Franchini *et al.* (2000).

Overall, the sensitivity analysis suggests that, for the climatic and basin soil conditions covered by the current sensitivity analysis, the *probability distribution of soil moisture*

content at the storm arrival time provides a unifying link between the perturbations to several of the parameters and their effects on the ffc. However, it should be emphasised that this result is conditioned by the climatic conditions considered, and the reference parameter sets for the simulation models. This conditioning will be relaxed in Franchini *et al.* (2000) by considering a wider range of climatic conditions, and by eliminating the dependence on the reference set. Indeed, in cases where wetter climatic conditions were simulated, it will be noted that soil moisture is not sufficient any more to explain the behaviour of the ffc, and other factors such as the spatial distribution of the soil moisture capacity and the extreme rainfall distributions for different durations have to be considered.

The routing component is represented by a lumped, linearized convective-diffusion equation whose parameters are C (celerity) and D (diffusivity), and a width function which provides a planar-geometric description of the channel network. Perturbations to C and D are reflected in the discharge value for a given return period, but the standardised ffc does not change. However, these results are strictly related to the assumption of linearity underlying the routing component which implies that all the non linear effects associated with the propagation of the flood waves through the flood plains are completely disregarded by this scheme.

The base length and the shape of the width function again alter the discharge for a given return period, but do not affect the curvature, and therefore, the standardised ffc. These effects are due to the different average path length that a drop of water has to follow to reach the basin outlet. However, many other physical aspects of the channel network (space variation of slopes, lengths, widths) are not included directly in the routing model used in this study.

To summarise, the effects of the routing component on the ffc observed in this study are tentative and further research related to the removal of the linear and lumped assumption is thus necessary. However, it is also clear that any linear routing approach (e.g. GIUH, Rodriguez-Iturbe and Valdes, 1979) cannot be used to explain regional variations of the curvature of the ffc.

Another result of the sensitivity analysis performed in this study is that perturbations to the climate and basin soil parameters move up/down or increase/decrease the curvature of the ffc but always leaving it with upward concavity on a Gumbel plot. The lower limit of the concavity is controlled by the curvature of the rainfall depth duration frequency curves. Downward concavity, sometimes observed in ffcs, can be due to the presence, in some zone upstream of the gauging station, of natural or man-made storage capacities, or other man-made devices that modify the flood wave above a certain discharge value (Mason *et al.*, 1988). But these features, as previously mentioned, were not included in the routing component of the rainfall-runoff model used and so that behaviour was never reproduced by the simulations.

Acknowledgements

The study was carried out under the following research programmes: FRAMEWORK (Flash-flood Risk Assessment under the iMpacts of land use changes and river Engineering WORKs: EC contract n° ENV4-CT97-0529), MURST-COFIN99 'Effetti climatici ed antropici sulla formazione delle piene', and CNR-GNDCI, contact n° 99.01417.PF42, project 'VAPI-RIVERS' (VAlutazione PIene-RIsposta di VERSante). The first author's PhD study was supported by the Ministry of Culture and Higher Education, Iran.

References

Adom, D.N., Bacchi, B., Brath, A. and Rosso, R., 1989. On the geomorphoclimatic derivation of flood frequency (peak and volume) at the basin and regional scale. In: *New directions for surface water modelling* M.L. Kavvas (Ed.). IAHS Publ. No., **181**, 165–176.

Anselmo, V., Galeati, G., Palmieri, S., Rossi, U. and Todini, E., 1996. Flood risk assessment using an integrated hydrological and hydraulic modelling approach: a case study, *J. Hydrol.*, **175**, 533–554.

Blazkova, S. and Beven, K., 1997. Flood frequency prediction for data limited catchments in the Czech Republic using a stochastic rainfall model and TOPMODEL. *J. Hydrol.*, **195**, 256–278.

Cadavid, L., Obeysekera, J.T.B. and Shen, H.W., 1991. Flood frequency derivation from kinematic wave. *J. Hydraul. Eng., ASCE*, **117**, 489–510.

Cameron, D., Beven, K., Tawan, J. and Naden, P., 2000. Flood frequency estimation by continuous simulation (with likelihood based uncertainity estimation). *Hydrol. Earth System Sci.*, **4**, 23–34.

Cowpertwait, P.S.P., 1994. A generalized point process model for rainfall. *Proc. Roy. Soc. Lond., Series A*, **447**, 23–37.

Cowpertwait, P.S.P., 1995. A generalized spatial-temporal model of rainfall based on a clustered point process. *Proc. Roy. Soc. Lond., Series A*, **450**, 163–175.

Cowpertwait, P.S.P., O'Connell, P.E., Metcalfe, A.V. and Mawdsley, J.A., 1996. Stochastic point process modelling of rainfall. II. Regionalisation and disaggregation. *J. Hydrol.*, **175**, 47–56.

Diaz-Granados, M.A., Valdes, J.B. and Bras, R.L., 1984. A physically-based flood frequency distribution. *Water Resour. Res.*, **20**, 995–1002.

Eagleson, P.S., 1972. Dynamic of flood frequency. *Water Resour. Res.*, **8**, 878–898.

Farquharson, F.A.K., Meigh, J.R. and Sutcliffe, J.V., 1992. Regional flood frequency-analysis in arid and semiarid areas, *J. Hydrol.*, **138**, 487–501.

Fiorentino, M. and Jacobellis, V., 2000. Non-linearity effects in the process of floods generation. *Mediterranean storm*, Proc. of the EGS Plinius Conference, Maratea, Italy, 14–16 October 1999, GNDCI Publ. n°2012, 269–276.

Franchini, M., 1996. Use of a genetic algorithm combined with a local search method for the automatic calibration of conceptual rainfall-runoff models. *Hydrol. Sciences J.*, **41**, 21–39.

Franchini, M. and O'Connell, P.E., 1996. An analysis of the dynamic component of the geomorphologic instantaneous unit hydrograph. *J. Hydrol.*, **175**, 407–428.

Franchini, M., Helmlinger, K.R., Foufoula-Georgiou, E. and Todini, E., 1996. Stochastic storm transposition coupled with rainfall-runoff modelling for estimation of exceedence probabilities of design floods, *J Hydrol.*, **175**, 511–532.

Franchini, M., Hashemi, A.M. and O'Connell, P.E., 2000. Climatic and basin factors affecting the flood frequency curve: PART II—A full sensitivity analysis based on the continuous

simulation approach combined with a factorial experimental design. *Hydrol. Earth System Sci.* **4**, 483–498.

Hashemi, A.M., O'Connell, P E., Franchini, M. and Cowpertwait, P.S.P., 1998. A simulation analysis of the factors controlling the shapes of flood frequency curves. *Hydrology in changing environment*, Vol. III, British Hydrological Society, 39–49.

Hebson, C. and Wood, E.F., 1982. A derived flood frequency distribution using Horton order ratios. *Water Resour. Res.*, **18**, 1509–1518.

Hosking, J.R.M. and Wallis, J.R., 1997. *Regional Frequency Analysis*, Cambridge University Press, pp 187.

Insititute of Hydrology, 1999. *Flood Estimation Handbook*, Wallingford, UK.

Jacobellis, V. and Fiorentino, M., 2000. Derived distribution of floods based on the concept of partial area coverage with a climatic appeal, *Water Resour. Res.*, **36** 469–482.

Mason, D.W., O'Connell, P.E. and Mawdsley, J.A., 1988. The effect of flood plain storage on the flood frequency curve. *Fifth IAHR International Symp. on Stochastic Hydraulics*, Birmingham, UK.

Naden, P.S., 1992. Spatial variability in flood estimation for large catchments: the exploitation of channel network structure. *J. Hydrol. Sci.*, **37**, 53–71.

NERC, 1975: *Flood studies report*. Nat. Environ. Res. Council, London, pp 174.

Rodriguez-Iturbe, I. and Valdés, J.B., 1979. The geomorphologic structure of hydrologic response, *Water Resour. Res.*, **15**, 1409–1420.

Shen, H.K., Knock, E.P. and Beven, K.J., 1990. On hydrological similarity, 3. A dimensionless flood frequency model using a generalised geomorphologic unit hydrograph and partial area runoff generation. *Water Resour. Res.*, **26**, 43–58.

Todini, E., 1996. The ARNO rainfall-runoff model. *J. Hydrol.*, **175**, 339–382.

Wood, E.F. and Hebson, C.S., 1986. On hydrological similarity, 1. Derivation of the dimensionless flood frequency curves, *Water Resour. Res.*, **22**, 1549–1554.

Zhao, R.J., 1977. *Flood forecasting method for humid region of China*. East China College of Hydraulic Engineering, Nanjing, China.